Topologically protected midgap states in complex photonic lattices

Henning Schomerus

Department of Physics, Lancaster University, Lancaster LA1 4YB, UK (h.schomerus@lancs.ac.uk)

Received April 16, 2013; accepted May 2, 2013;
posted May 6, 2013 (Doc. ID 188919); published May 27, 2013

One of the principal goals in the design of photonic crystals is the engineering of band gaps and defect states. Here I describe the formation of topologically protected localized midgap states in systems with spatially distributed gain and loss. These states can be selectively amplified, which finds applications in the beam dynamics along a photonic lattice and in the lasing of quasi-one-dimensional photonic crystals. © 2013 Optical Society of America

OCIS codes: (130.2790) Guided waves; (140.3410) Laser resonators; (160.5293) Photonic bandgap materials.
http://dx.doi.org/10.1364/OL.38.001912

Since the inception of the field [1,2], the design of photonic crystals with band gaps and defect states has been facilitated by drawing analogies to condensed matter systems. An impetus for such endeavors is provided by the discovery of topological insulators and superconductors, systems that occur in distinct configurations that cannot be connected without closing a gap in the band structure and consequently display robust surface and interface states [3]. Recent works have started to transfer concepts of band-structure topology to the photonic setting. Thus far, this has opened up avenues for unidirectional transport [4,5], adiabatic pumping of light [6], and the creation of photonic Landau levels [7,8], as well as the creation of bound and edge states via dynamic modulation in the time domain [9,10].

The practical utility of topological concepts in photonics will depend much on the robustness versus absorption and amplification. Remarkably, as shown here for a complex version of the Su–Schrieffer–Heeger (SSH) model [11], such robustness can be demonstrated for a photonic realization of topologically protected midgap states, localized at an interface in the interior of the system. Under the influence of spatially distributed gain and loss [12–14], these states not only maintain their topological characteristics but also acquire desirable properties —the midgap states can be selectively amplified without affecting the extended states in the system. This sets these states apart from conventional defect states and can be utilized in beam manipulation and lasing.

The SSH model was originally introduced to describe fractionalized charges in polyacetylene, where exponentially localized midgap states form at defects in the dimerization pattern [11]. I consider a version [the complex Su–Schrieffer–Heeger (cSSH) model, shown in Fig. 1] that applies to photonic lattices and crystals and incorporates distributed loss and gain [12–14]. The original SSH model consists of a tight-binding chain with alternating coupling constants t_a and t_b (for specificity let us assume $t_a > t_b > 0$) and a defect in this sequence that supports the topologically protected midgap state (see Fig. 1). The fundamental unit cell is composed of two sites (labeled A and B) with amplitudes $\psi_n^{(A)}$ and $\psi_n^{(B)}$, where the integer n enumerates the unit cells. The cSSH model incorporates effects of loss and gain via a staggered complex onsite potential $i\gamma_A = i\bar{\gamma} + i\gamma$ on the A sites and $i\gamma_B = i\bar{\gamma} - i\gamma$ on the B sites. The coupled-mode equations read

$$\varepsilon\psi_n^{(A)} = i\gamma_A\psi_n^{(A)} + t'_n\psi_{n-1}^{(B)} + t_n\psi_n^{(B)}, \tag{1a}$$

$$\varepsilon\psi_n^{(B)} = i\gamma_B\psi_n^{(B)} + t_n\psi_n^{(A)} + t'_{n+1}\psi_{n+1}^{(A)}, \tag{1b}$$

where t_n is the intradimer coupling and t'_n is the interdimer coupling. The infinitely periodic system exists in two configurations—a configuration α where $t_n = t_a$ and $t'_n = t_b$, and a configuration β where the values are interchanged such that $t_n = t_b$ and $t'_n = t_a$. These configurations are associated with Bloch Hamiltonians

$$\mathscr{H}(k) = \begin{pmatrix} i\gamma_A & f(-k) \\ f(k) & i\gamma_B \end{pmatrix}, \qquad f(k) = \begin{cases} t_a + t_b e^{ik} & (\alpha) \\ t_b + t_a e^{ik} & (\beta) \end{cases}, \tag{2}$$

delivering identical dispersion relations

$$\varepsilon_\pm(k) = i\bar{\gamma} \pm \sqrt{t_a^2 + t_b^2 + 2t_a t_b \cos k - \gamma^2} \tag{3}$$

for extended states with dimensionless wavenumber k.

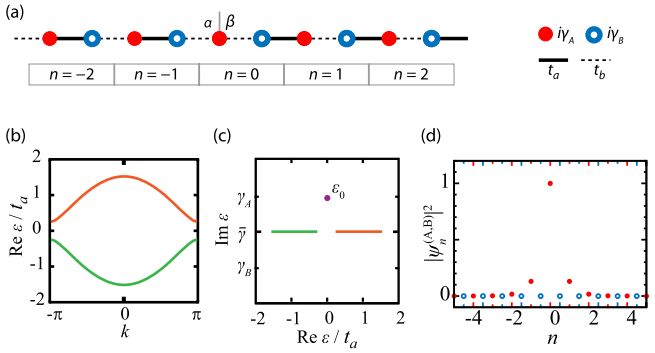

Fig. 1. (a) Complex Su–Schrieffer–Heeger (cSSH) chain with alternating couplings t_a and t_b and alternating imaginary onsite potential $i\gamma_A = i(\bar{\gamma} + \gamma)$ and $i\gamma_B = i(\bar{\gamma} - \gamma)$ (describing loss or gain). For $n < 0$ the system is in the α configuration; for $n > 0$ it is in the β configuration. (b) Dispersion $\mathrm{Re}\,\varepsilon(k)$ of the extended states, for $t_b = 0.6t_a$ and $\gamma = 0.3t_a$. These states have $\mathrm{Im}\,\varepsilon(k) = \bar{\gamma}$. (c) Dispersion in the complex eigenvalue plane, including the midgap state at $\varepsilon_0 = i\gamma_A$, which forms due to the coupling defect. (d) The midgap state is exponentially localized and confined to the A sublattice.

In the original SSH model with $\bar{\gamma} = \gamma = 0$, this results in two bands, symmetrically arranged about $\varepsilon = 0$ and separated by a gap $\Delta = 2(t_a - t_b)$. In the cSSH model these bands are shifted into the complex plane, corresponding to decaying states if $\mathrm{Im}\,\varepsilon < 0$ and amplified states if $\mathrm{Im}\,\varepsilon > 0$. However, this shift is uniform if $|\gamma| < \gamma_c = \Delta/2$, which is imposed henceforward. Under this condition, all extended states experience the same overall gain ($\bar{\gamma} > 0$) or loss ($\bar{\gamma} < 0$). In the particular case $\bar{\gamma} = 0$ of balanced loss and gain, the dispersion remains real (which can be explained by the symmetry $\sigma_x[\mathscr{H}(k)]^*\sigma_x = \mathscr{H}(k)$ with Pauli matrix σ_x [15,16]).

The midgap state appears when the two configurations are coupled together. In Fig. 1(a), the system is in the α configuration for $n < 0$ and in the β configuration for $n \geq 0$, joined by a coupling defect. The spectrum [Figs. 1(b) and 1(c)] consists of extended states from the two bands, plus an additional state at $\varepsilon_0 = i\gamma_A$. According to Eqs. (1), this value admits an exponentially localized solution with $\psi_n^A = (-t_b/t_a)^{-|n|}$ and $\psi_n^B = 0$ [Fig. 1(d)]. In the original SSH model the midgap state sits at $\varepsilon_0 = 0$. In the cSSH model the midgap state breaks the symmetry of the spectrum—the midgap state is more stable than the extended states if $\gamma > 0$, and less stable if $\gamma < 0$.

Let us first consider the manifestation of the midgap state in the beam propagation along a photonic lattice, composed of single-mode waveguides as shown in Fig. 2. Experimentally, such lattices can be realized using optical fibers, quantum wells, or femtosecond laser-writing techniques, producing in all cases arrays of waveguides aligned along the propagation direction z [17]. In this setting the parameters γ_A and γ_B describe the intrinsic propagation constants of the waveguides, which are lossy if $\gamma_{A,B} < 0$ and amplifying if $\gamma_{A,B} > 0$. The couplings take the values t_a and t_b, depending on whether the spacing between the waveguides is a or b, respectively, and the midgap state now arises from a defect in an alternating spacing sequence. Modes with $\mathrm{Im}\,\varepsilon > 0$ exponentially increase along the propagation direction z, while those with $\mathrm{Im}\,\varepsilon < 0$ decay.

I now set $\gamma_A = 0$ and $\gamma_B = -2\gamma < 0$, corresponding a setup with passive A sites and lossy B sites. The midgap state is then lossless ($\varepsilon_0 = 0$), while the extended states decay uniformly according to $\mathrm{Im}\,\varepsilon = \bar{\gamma} = -\gamma < 0$. Figure 2 illustrates the beam propagation in a lattice of 101 fibers and a spacing defect in the center of the system. Figure 2(a) depicts the arrangement of the fibers close to the center of the sample. In Fig. 2(b), a broad wave packet is fed into the lattice with $t_b = 0.2t_a$ and $\gamma = 0.05t_a$. After a short time, the midgap state is populated and propagates without attenuation. In Fig. 2(c), the light is fed into a single A fiber close to the center of the sample. Again, the midgap state is populated; it is now less localized because here I set $t_b = 0.6t_a$. In Fig. 2(d), the light is fed into a neighboring B fiber of the same lattice. The beam quickly subsides as the midgap state is not populated. Figures 2(e) and 2(f) demonstrate the feasibility of adiabatic light pumping [6] in a lattice where the interface gradually shifts by five unit cells to the right. In the transient region the couplings t_n and t_n' interpolate linearly between t_a and t_b, with $t_b = 0.2t_a$ and $\gamma = 0.1t_a$. Note that the shift of the beam is opposite to the displacement of the individual waveguides.

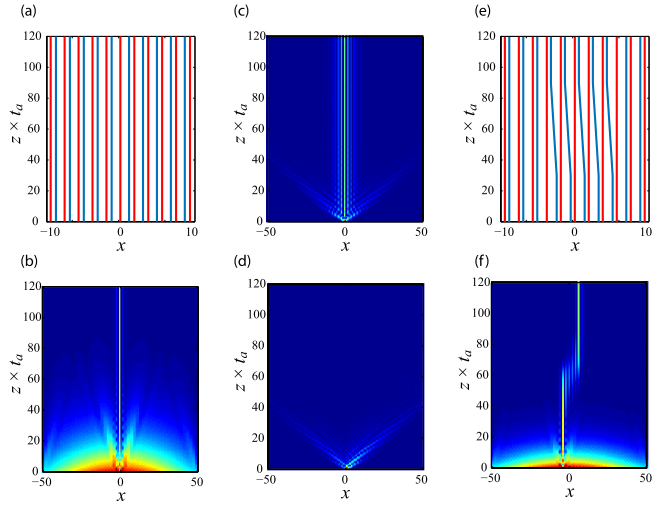

Fig. 2. (a) Realization of the cSSH model in a photonic lattice of single-mode waveguides with intrinsic propagation constants γ_A and γ_B as well as alternating spacings a and b, and a defect in that spacing sequence (around $x = 0$). (b) Beam propagation of an initially broad wave packet in a lattice of 101 waveguides with $t_b = 0.2t_a$, $\gamma_A = 0$, and $\gamma_B = -0.1t_a$. (c), (d) Beam propagation with light fed into an A or B fiber close to $x = 0$, for a lattice with $t_b = 0.6t_a$, $\gamma_A = 0$, and $\gamma_B = -0.1t_a$. (e) Adiabatic pumping of light: waveguide geometry close to the center of the system. (f) Beam propagation in a lattice of 101 waveguides, with $t_b = 0.2t_a$, $\gamma_A = 0$, and $\gamma_B = -0.2t_a$.

These results generalize to systems with $\gamma_A \neq 0$. At fixed γ, this implies a z-dependent intensity scaling $\exp(2\gamma_A z)$. When such a system is confined in the z direction, it is useful to apply the slowly varying envelope approximation and interpret the eigenvalues of the cSSH model as the mode frequencies $\omega_i = \varepsilon_i + \Omega$ around a large central frequency Ω. In active realizations with $\gamma_A = \bar{\gamma} + \gamma > 0 > \gamma_B = \bar{\gamma} - \gamma$, $|\gamma| < \gamma_c$, the midgap state is then amplified in the time domain, while the extended states all decay. This provides a topological realization of microlasing with distributed gain and loss [18–20]. Figure 3(a) illustrates how such a system could be realized using an arrangement of amplifying and absorbing (or passive) regions separated by gaps of alternating length. Figures 3(b) and 3(c) demonstrate the applicability of cSSH predictions for an implementation of the laser in a dielectric medium with refractive index $n_A = 2 - 0.01i$ in the amplifying parts and $n_B = 2 + 0.01i$ in the absorbing parts of the system. Midgap states form in the gaps between the lowest-lying bands, which is illustrated here for bands 8 and 9. The state is localized in the amplifying regions, and its frequency lies much higher up in the complex plane than those of the extended states.

Let us finally discuss how the features of the midgap state relate to the topological properties of the cSSH model. I write the eigenvectors of Hamiltonian (2) as

$$\varphi(k) = N\begin{pmatrix} f(-k) \\ \varepsilon(k) - i\gamma_A \end{pmatrix} \equiv \begin{pmatrix} \varphi^{(A)}(k) \\ \varphi^{(B)}(k) \end{pmatrix}, \tag{4}$$

where N is the normalization constant. Each extended state can then be associated with a pseudospin vector

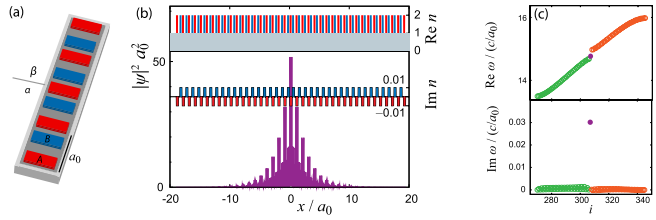

Fig. 3. (a) Realization of the cSSH model in a quasi-one-dimensional photonic laser with a staggered arrangement of active (A) and lossy components (B) in a unit cell of size a_0. (b) Midgap state in a dielectric medium with regions of refractive index $n_A = 2 - 0.01i$ (gain) and $n_B = 2 + 0.01i$ (loss). The regions have lengths $a_0/3$ and are separated by gaps (refractive index $n = 1$) of alternating size $a_0/12$ and $a_0/4$ (system length 40 a_0). The state is predominantly localized in the gain medium. (c) Bands 8 and 9 of the system, in increasing order of Re ε_i. The depicted midgap state has index $i = 308$.

$$\mathbf{S} = \langle(\sigma_x, \sigma_y, \sigma_z)\rangle = (S_x, S_y, S_z). \tag{5}$$

From Eq. (5), $S_z = 0$ as long as $|\gamma| < \gamma_c$, while

$$S_x + iS_y \propto (\varepsilon(k) - i\gamma_A)f(k) \equiv g(k). \tag{6}$$

In the α configuration, over a sweep through the Brillouin zone, the function $g(k)$ does not encircle the origin of the complex plane; the pseudospin therefore librates and traces out an arc (winding number 0, topological phase 0). In the β configuration $g(k)$ encircles the origin; the pseudospin therefore rotates and traces out a circle (winding number 1, topological phase π). Combined with the chiral symmetry $\sigma_z[\mathscr{H}(-k)]^*\sigma_z = -\mathscr{H}(k)$, the presence of the defect must then result in a midgap state [21]. Due to the localization on the A sublattice, this state possesses a fully polarized pseudospin $\mathbf{S} = (0, 0, 1)$ and inherits the complex potential on this sublattice, which thus determines its eigenvalue $\varepsilon_0 = i\gamma_A = i\bar{\gamma} + i\gamma$. This state is topologically protected against hopping disorder, while the finite gap also provides some robustness against onsite disorder.

In conclusion, photonic systems can exhibit exponentially localized, topologically protected midgap states whose properties are controlled via distributed loss and gain. Such states can be induced in the beam propagation through photonic lattices, where they provide a platform for adiabatic pumping of light, and in photonic crystal lasers with inhomogeneous gain, where they exhibit selective level amplification. Remarkably, the midgap states maintain their topological protection even though the loss and gain renders the underlying Hamiltonian non-Hermitian and breaks the time reversal symmetry of the system. This demonstrates the utility of topological concepts in genuinely photonic settings.

I gratefully acknowledge discussions with Hui Cao, Yaron Bromberg, Ramy El-Ganainy, and Jan Wiersig.

References

1. E. Yablonovitch, Phys. Rev. Lett. **58**, 2059 (1987).
2. S. John, Phys. Rev. Lett. **58**, 2486 (1987).
3. M. Z. Hasan and C. L. Kane, Rev. Mod. Phys. **82**, 3045 (2010).
4. Z. Wang, Y. Chong, J. D. Joannopoulos, and M. Soljačić, Nature **461**, 772 (2009).
5. M. Hafezi, E. A. Demler, M. D. Lukin, and J. M. Taylor, Nat. Phys. **7**, 907 (2011).
6. Y. E. Kraus, Y. Lahini, Z. Ringel, M. Verbin, and O. Zilberberg, Phys. Rev. Lett. **109**, 106402 (2012).
7. H. Schomerus and N. Yunger Halpern, Phys. Rev. Lett. **110**, 013903 (2013).
8. M. C. Rechtsman, J. M. Zeuner, A. Tünnermann, S. Nolte, M. Segev, and A. Szameit, Nat. Photonics **7**, 153 (2013).
9. K. Fang, Z. Yu, and S. Fan, Nat. Photonics **6**, 782 (2012).
10. T. Kitagawa, M. A. Broome, A. Fedrizzi, M. S. Rudner, E. Berg, I. Kassal, A. Aspuru-Guzik, E. Demler, and A. G. White, Nat. Comms. **3**, 882 (2012).
11. W. P. Su, J. R. Schrieffer, and A. J. Heeger, Phys. Rev. Lett. **42**, 1698 (1979).
12. K. G. Makris, R. El-Ganainy, D. N. Christodoulides, and Z. H. Musslimani, Phys. Rev. Lett. **100**, 103904 (2008).
13. A. Guo, G. J. Salamo, D. Duchesne, R. Morandotti, M. Volatier-Ravat, V. Aimez, G. A. Siviloglou, and D. N. Christodoulides, Phys. Rev. Lett. **103**, 093902 (2009).
14. C. E. Rüter, K. G. Makris, R. El-Ganainy, D. N. Christodoulides, M. Segev, and D. Kip, Nat. Phys. **6**, 192 (2010).
15. M. C. Zheng, D. N. Christodoulides, R. Fleischmann, and T. Kottos, Phys. Rev. A **82**, 010103 (2010).
16. H. Ramezani, D. N. Christodoulides, V. Kovanis, I. Vitebskiy, and T. Kottos, Phys. Rev. Lett. **109**, 033902 (2012).
17. D. N. Christodoulides, F. Lederer, and Y. Silberberg, Nature **424**, 817 (2003).
18. H. Schomerus, Phys. Rev. Lett. **104**, 233601 (2010).
19. S. Longhi, Phys. Rev. A **82**, 031801 (2010).
20. Y. D. Chong, L. Ge, and A. D. Stone, Phys. Rev. Lett. **106**, 093902 (2011).
21. S. Ryu and Y. Hatsugai, Phys. Rev. Lett. **89**, 077002 (2002).